Technical Notes

TECHNICAL NOTES are short manuscripts describing new developments or important results of a preliminary nature. These Notes cannot exceed 6 manuscript pages and 3 figures; a page of text may be substituted for a figure and vice versa. After informal review by the editors, they may be published within a few months of the date of receipt. Style requirements are the same as for regular contributions (see inside back cover).

Performance and Characteristics of Cylindrical Resonator Igniters

R. A. Neemeh* and M. N. Elabdin†
Concordia University, Montreal, Canada

Introduction

THE objective of this study was to improve the performance of the original resonator[1,2] by eliminating its operational dependence on the jet pressure ratio, and to find the conditions required for maximum pressure amplitudes through a detailed parametric study. Four parameters were studied, namely, the disk diameter, the cylindrical chamber width, and disk and plug positions.

The new device was designed based on Sprenger's,[3] rather than Hartmann's tube principles, where the center core of the jet is weakened by a trip wire placed across the jet. Sprenger's tube works with a wide range of jet pressure ratios and with both subsonic and supersonic jets. In the new model, the jet is subsonic, which allows for a given air supply, the use of larger nozzle widths while maintaining steady jet and uniform flow conditions for a considerable time period. The effect of the four parameters on its operation was studied via pressure and temperature measurements. The symmetry and shape of the converging shock were observed from the spark Schlieren photographs taken near the geometric center of the device. A full description of the apparatus is presented next, followed by experimental results and conclusions.

Experimental Apparatus

The present work proposes an alternate model to that described earlier,[1] and operates at a wide range of jet stagnation pressures, producing converging shock waves with high degrees of circular symmetry. The shape of the axisymmetric model was obtained by rotating the upper half of the two-dimensional model (Sprenger tube), shown in Fig. 1a, about axis A-A. A schematic of the resonator used is shown in Fig. 1b. It consists of a cylindrical plenum chamber supplied by 20 1-in.-diam inlets. The latter are connected to a 6-m^3 tank filled with air at a pressure of 830 kPa. A narrow slit with a 6-mm rounded entrance in the inner wall serves as a nozzle. The nozzle jet is surrounded on one side by a disk with a 30-deg chamfer and on the other side by a plug. The position of the disk and the plug may be adjusted by threaded rods in order to control the width of the cylindrical cavity. Here, the plug acts as the trip wire used in the Sprenger tube case, to weaken the jet close to its surface so that the outflow and the oscillations can be maintained at subsonic jet conditions.

Received Dec. 6, 1989; revision received Feb. 2, 1990; accepted for publication April 17, 1990.

*Associate Professor, Department of Mechanical Engineering. Member AIAA.

†Research Associate, Department of Mechanical Engineering.

An enlarged portion of the cylindrical cavity is also presented in Fig. 1b to show the most important parameters affecting the operation of the device. The first two parameters are the disk position S_d and the plug position S_p. When both of these parameters are equal to zero, the disk and plug are said to be in the flush position. Larger values of S_p in the cylindrical resonator increase the depression in the velocity near the plug surface and are, therefore, equivalent to the increase in the trip wire's size in the Sprenger tube case. Due to the widening of the jet as it approaches the center, an adjust-

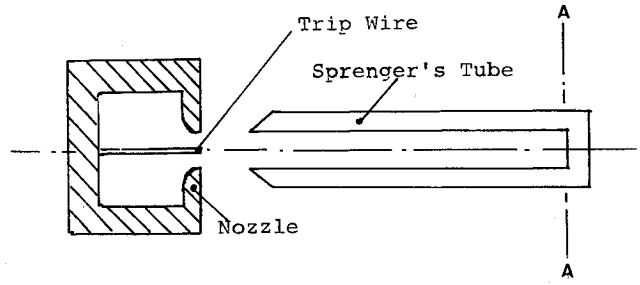

Fig. 1a Schematic of a modified H-S tube.

A Plenum Chamber
B Air Inlet
C Nozzle Ring
D Threaded Rod
E Screen
F Slotted Plate
G Locking Ring
H Disc and Mirror
I Cylindrical Cavity
J Optical Path
K Circular Jet
L Plug, Glass Window

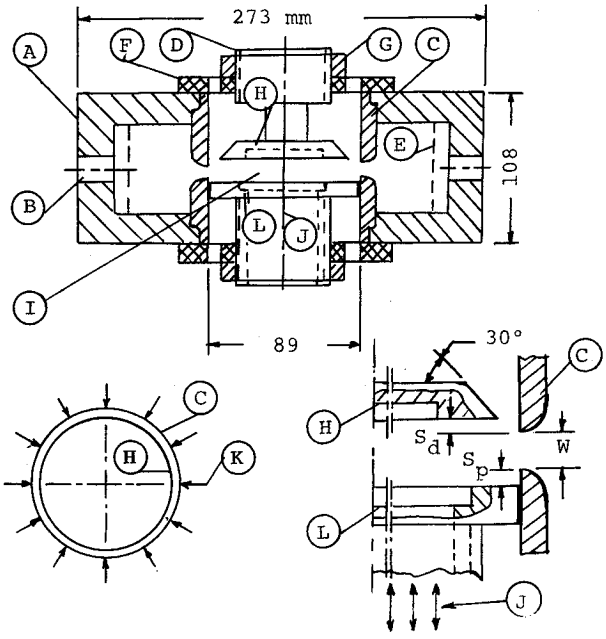

Fig. 1b Schematic of the cylindrical resonator.

Table 1 Optimum disk and plug positions for various disk diameters

Disk diameter, mm	S_d, mm	S_p, mm
64	0.3	1.6
69	0.3	1.6
74	1.3	1.3
79	0.3	0.6

ment for the disk position S_d is essential in the present case. The third and fourth parameters are the nozzle width w and the disk diameter. Note that the width of the cylindrical chamber is a sum of all three parameters, namely, the nozzle width, S_p, and S_d. In the present work, the nozzle diameter is fixed at 89 mm.

The effect of the four parameters on the operation of the new model is presented in details in the next section.

Results and Discussion

The various tests performed were piezoelectric pressure measurements at the geometric center of the cylindrical cavity, spark schlieren photography of the converging shock at both design and off-design conditions, and temperature measurements.

The pressure measurements were carried out to determine, for any given disk diameter, the disk and plug positions required for maximum pressure amplitudes. The results are tabulated in Table 1 for four disk diameters of 64, 69, 74, and 79 mm. As noted in Table 1, S_p increases with the decrease in disk diameter. For the 79-mm disk diameter, S_p is 0.6 mm. At smaller disk diameters, the magnitude of the depression in the jet velocity near the plug surface decreases. To increase the depression, the plug was placed at a larger distance (1.6 mm) from the nozzle exit plane for the smallest disk diameter of 64 mm.

With both disk and plug placed at the optimum positions, given in Table 1, detailed pressure measurements were carried out for various jet stagnation pressures (P_{oj}). The latter was measured by means of a gauge mounted on the plenum chamber. The pressure amplitude (Δp) of the oscillatory flow was measured from the oscilloscope traces obtained using a *Pcb* piezoelectric transducer, placed at the geometric center of the device. The results are presented in Fig. 2, together with those previously obtained from a simple Hartmann-Sprenger (H-S) tube. For a 64-mm disk, the pressure amplitudes were found to be smaller than those corresponding to the simple H-S tube. For larger disk diameters, higher pressure amplitudes were noted. The highest amplitude was recorded with the 74-mm disk, at a jet Mach number of 0.985, and found to be 1.8 times that obtained with a Hartmann-Sprenger tube. This is close to the value of 1.87, obtained by using stepped tubes with large area contractions[4] and the value of 2 obtained by the acoustic theory. For the 74-mm disk, the frequency of oscillation was 2.78 Kcps, which is 21% lower than that of the acoustic frequency of 3.53 Kcps, with $c = 342$ m/s.

The effects of the jet width and, consequently, the boundary layer on the operation of the device were also investigated. Three nozzle widths of 2.5, 3.8, and 5.1 mm were tested. The results are shown in Fig. 3. For a jet width of 2.5 mm, no noticeable oscillations were observed beyond a jet Mach number of 0.83. This phenomenon was not present for the other two jet widths tested. The highest pressure amplitude was recorded with the 5.1-mm nozzle, which corresponds to a cylindrical chamber radius of about 10 times its width. This is similar to the condition for minimal boundary-layer interference,[6] in the simple Hartmann-Sprenger tube case.

To examine the symmetry of the converging shocks, spark schlieren photographs were taken near the geometric center of the device, which was set at maximum operating conditions. The schlieren system used consisted of a 2 KV spark source, a double-headed parabolic mirror, a vertical knife edge, and an

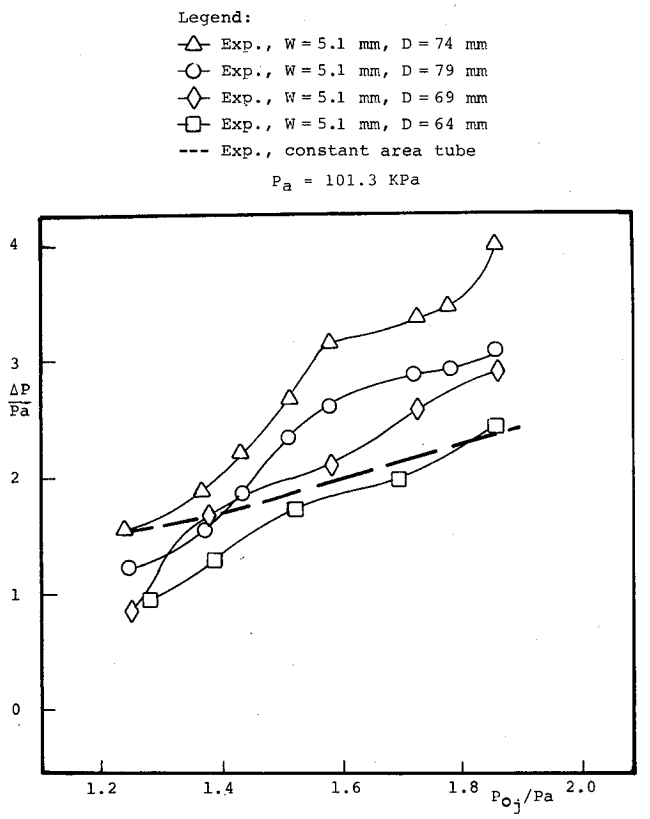

Fig. 2 Experimental values of the pressure amplitude.

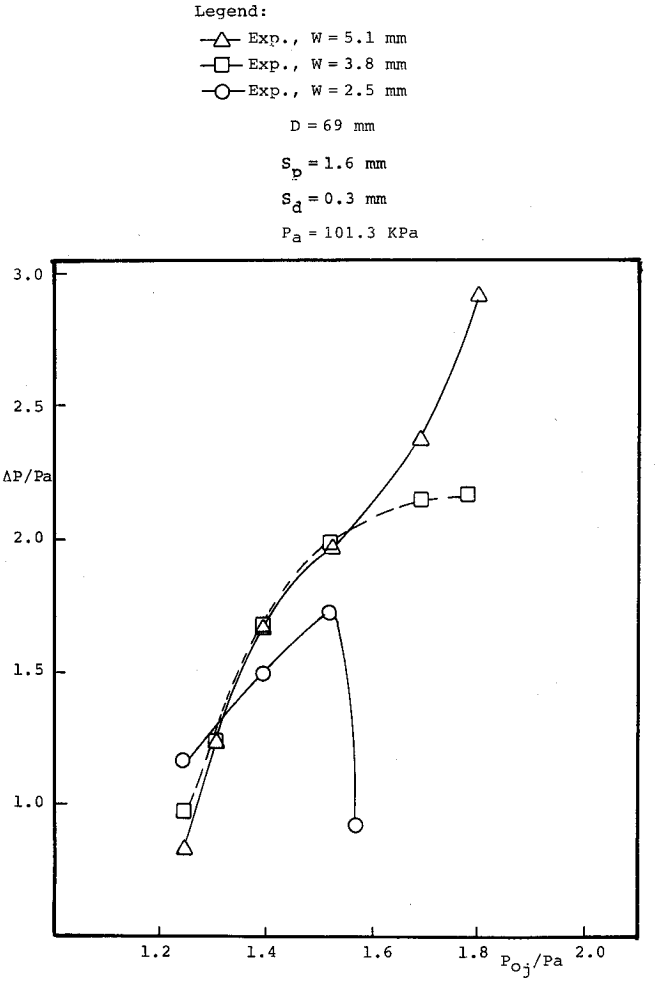

Fig. 3 Pressure amplitudes for various nozzle widths.

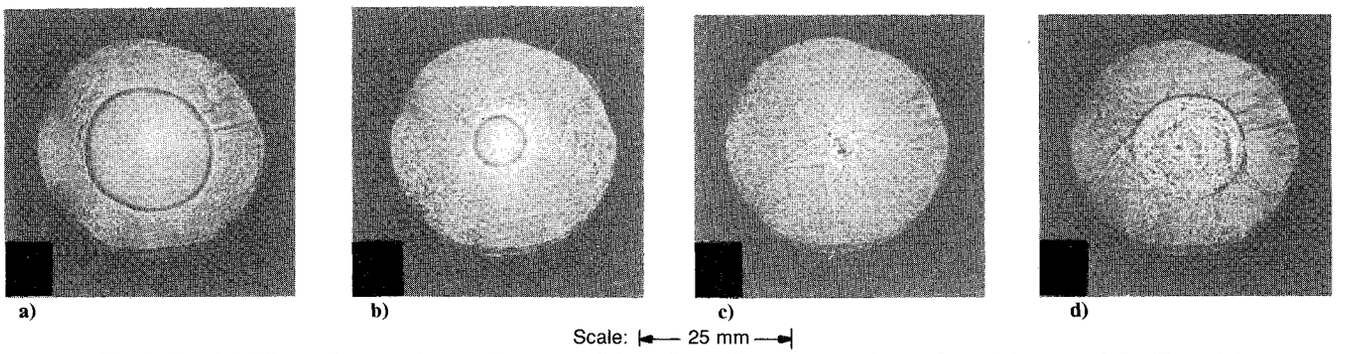

Fig. 4 Spark Schlieren photographs at optimum conditions: D = 74 mm, S_d = 1.3 mm, S_p = 1.3 mm, and P_{oj}/P_a = 1.6.

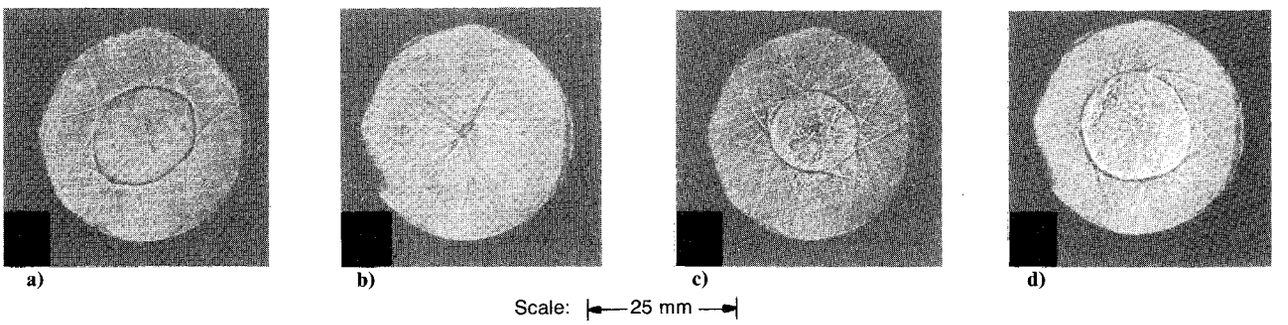

Fig. 5 Spark Schlieren photographs at optimum conditions but without the screen in the plenum chamber, P_{oj}/P_a = 1.6.

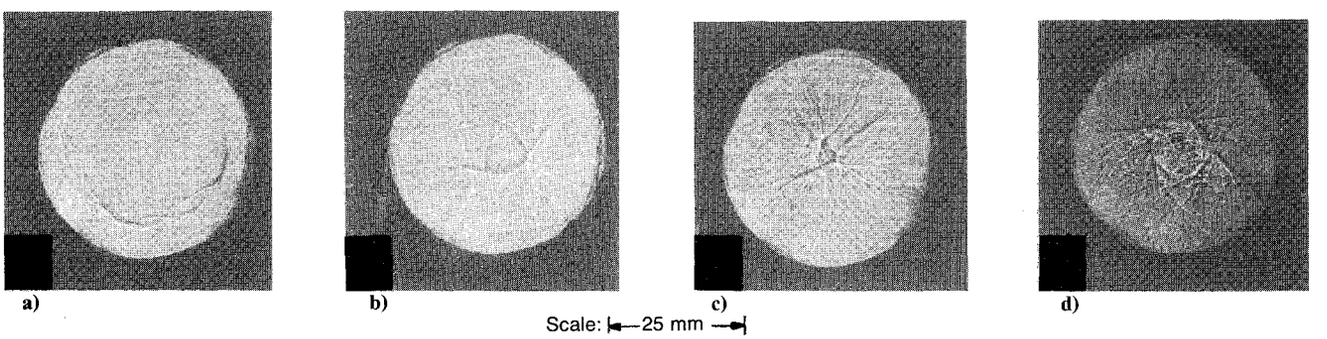

Fig. 6 Spark Schlieren photographs: D = 74 mm, S_d = 1.3 mm, S_p = 0.64 mm, P_{oj}/P_a = 1.6, without the screen.

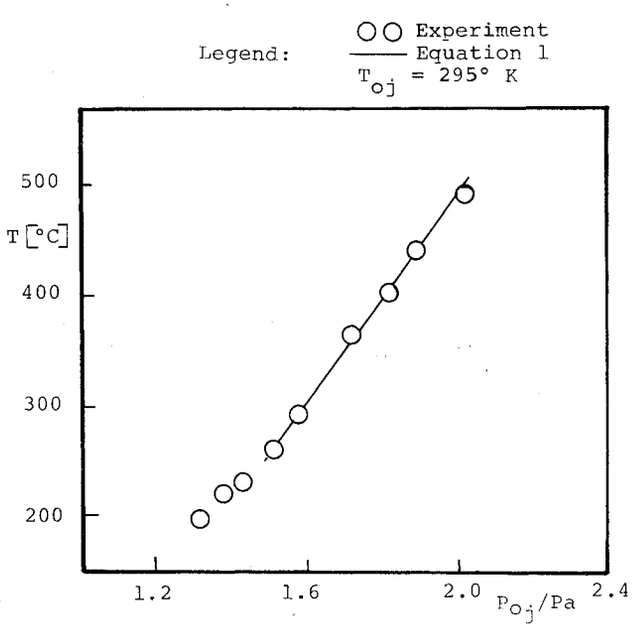

Fig. 7 Equilibrium temperatures at the geometric center of the cylindrical cavity.

open shutter camera. For viewing purposes, a plane mirror and a glass window were placed at the center of the disk and plug, respectively (see Fig. 1b). A set of photographs are shown in Fig. 4 for a disk diameter of 74 mm and a jet pressure ratio of 1.6. As noted, the shock symmetry has improved in comparison to those obtained with the old apparatus. Figures 4a and 4b show the converging shock; Figs. 4c and 4d show the expanding one. Another series of photographs were taken with the same operating conditions as before but without the screen (Fig. 5). The shock in this case is seen with multiple fronts that later merge into one, but with a large number of transverse waves. The latter, created during shock convergence, interact with the expanding cylindrical shock, as shown in Figs. 4c and 4d. Without the screen and with the plug placed at a distance of 0.64 mm, the converging shock was not cylindrical, as noted in Fig. 6a. The upper part of the shock was initially weaker than the lower part. This resulted in weaker oscillations due to nonuniformity in the jet.

To complete this investigation, temperature measurements were carried out with a 0.13-mm chromel-alumel thermocouple placed at the geometric center. The apparatus was set at optimum operating conditions with a disk diameter of 74 mm. The thermocouple was connected to a digital temperature indicator (Omega Model 2809 C). For jet stagnation pressures ($1.3 \leq P_{oj}/P_a \leq 2.1$), steady-state temperatures were recorded. The results, presented in Fig. 7, show a steady increase

in temperature as the jet pressure ratio increases to its maximum possible reliable limit ($P_{oj}/P_a = 2.1$). Beyond this limit it was hard to keep the supply pressure constant long enough to have reliable results. For jet stagnation pressures ($1.43 \leq P_{oj}/P_a \leq 2.1$), the following linear empirical equation was obtained:

$$T = 230 + 444\,(P_{oj}/P_a - 1.43)\,C$$

At higher pressures, the cylindrical resonator is expected to yield higher temperatures, as suggested by this equation. This was not verified experimentally, due to the difficulties encountered in maintaining the jet pressure long enough to obtain a temperature reading.

Concluding Remarks

A new and improved axisymmetric resonator was introduced and tested. The results were compared with those obtained using the original model and the following conclusions were drawn:

1) Highly symmetrical implosions are possible to obtain, and depend not only on the symmetry of the device but on its four parameters studied here, namely, the disk diameter, nozzle width, and disk and plug positions. For a given nozzle diameter and width, there exists, for every disk diameter, an optimum position for both the disk and the plug. For the 89-mm nozzle diameter and the 5.1-mm nozzle width, the optimum plug and disk positions are given in Table 1.

2) Resonant oscillations can be obtained for a wide range of jet stagnation pressures and not restricted to a single value, as in the original model. The higher the jet pressure, the higher is the pressure amplitude, as shown in Fig. 4.

3) To minimize the effects of the boundary layers, the disk diameter to cylindrical cavity width ratio should be less than 10. Smaller nozzle and cavity widths were found to weaken the oscillations, which become almost nonexistent at higher pressures.

4) The steady-state temperatures were found to vary linearly with the jet stagnation pressures. For jet stagnation pressures ($1.43 \leq P_{oj} \leq 2.1$), a linear empirical equation was obtained. These values are about five times those measured with a logarithmic spiral resonance tube,[5] thus making the proposed model a better ignitor over any of the existing ones. Future work should include the use of different gases, such as helium and hydrogen, which were previously found to yield temperatures about six times that obtained with air,[6] as well as testing of the new model for its ability to ignite various gaseous mixtures.

Acknowledgment

The present work is supported by the Natural Sciences and Engineering Research Council of Canada under Grant A-4206.

References

[1]Wu, J. H. T., Ostrowski, P. P., Neemeh, R. A., and Lee, P., "Experimental Investigation of a Cylindrical Resonator," *AIAA Journal,* Vol. 12, Aug. 1974, pp. 1076–1078.

[2]Wu, J. H. T., Ostrowski, P. P., and Neemeh, R. A., "Cylindrical Shock Waves in a Resonator," *Proceedings of the 10th International Symposium on Shock Tubes and Waves*, Shock Tube Research Society, Kyoto, Japan, July 14–16, 1975, pp. 141–148.

[3]Sprenger, M., "Uber Thermische Effekte in Rezonanzrohren," Mitt. Inst. Aerodynamik, Zurich, Switzerland, No. 21, 1954, pp. 18–35.

[4]Neemeh, R. A., and Skarzynska, B., "Shock and Pressure Amplification in a Stepped Hartmann-Sprenger's Tube," *CAS Journal,* Vol. 34, No. 1, March 1988, pp. 48–54.

[5]Neemeh, R. A., Ostrowski, P. P., and Wu, J. H. T., "Thermal Performance of a Logarithmic-Spiral Resonance Tube," *AIAA Journal,* Vol. 22, Dec. 1984, pp. 1823–1825.

[6]Rakowsky, E. L., Corrado, A. A., and Marchesse, V. P., "Fluidic Explosive Initiator," Sixth Cranfield Fluidics Conf., BHRA Fluid Engineering, Cranfield, Bedford, England, UK, March 26–28, 1974, Paper H4, pp. 29–41.

Numerical Simulation of the Transient Ignition Regime of a Turbulent Diffusion Flame

D. Veynante,* F. Lacas,† and S. M. Candel‡
Ecole Centrale des Arts et Manufactures, Chatenay-Malabry, France F92295

I. Introduction

MANY recent studies of turbulent combustion are based on flamelet models in which the reaction zone is treated as a collection of laminar flame elements (flamelets) embedded in the turbulent flow (Marble and Broadwell,[1] Peters,[2,3] Bray[4]). An advantage of this concept is that it essentially decouples complex chemistry calculations from the turbulent flow description. Chemical kinetics and transport properties may be treated separately in a local flamelet analysis and then included in the calculation of the turbulent flowfield. Two different formulations of these flamelet models are generally available: one for turbulent premixed flames, the other for turbulent diffusion flames. However, in some situations, premixed and nonpremixed flame elements may co-exist in the same flow. This is the case, for example, in the stabilization of diffusion flames or during the ignition phase of a cryogenic rocket engine. In a first step, the cold reactants, fuel and oxidizer, mix to form a premixed fluid. Then, when ignition occurs due to some external process such as autoignition, by mixing with a hot gas stream or spark ignition, a premixed flame is formed. All premixed reactants are eventually consumed and a stabilized diffusion flame takes over. Combustion in a diesel engine also begins with the ignition of a premixed flame and ends with a diffusion flame. It appears that such a situation is not adequately described with classical flamelet models. A combined flamelet representation, based on the coherent flame model initially derived by Marble and Broadwell,[1] accounting for premixed and nonpremixed flame regimes is tested to describe the unsteady reactive flow configurations.

II. Combined Flamelet Model

The combined model devised in this article employs the basic assumptions of the coherent flame model of Marble and Broadwell. Details of this model may be found in Ref. 1, as well as in Veynante et al.,[5,6] Lacas et al.,[7] or Darabiha et al.[8] The turbulent reactive flow is described as a collection of laminar flamelets which are convected and distorted by the turbulent motion but retain an identifiable structure. In this sense, the reaction sheets remain "coherent." The basic model combines the following elements: 1) a set of dynamic equations and closure rules describing the turbulent flow, 2) a local model for the laminar flame elements taking into account the effect of strain and providing the consumption rates per unit flame area, V_{D_i}, and 3) a balance equation for the flame area per unit volume Σ.

The mean consumption rates of the main species are then obtained from Σ and V_{D_i} according to:

$$\dot{W} = \rho\, V_{D_i} \Sigma \tag{1}$$

Received Aug. 7, 1989; revision received Jan. 2, 1990.

*Research Fellow, Laboratoire EM2C, CNRS. Member AIAA.
†Research Fellow, Laboratoire EM2C, CNRS.
‡Professor, Laboratoire EM2C, CNRS. Member AIAA.